JCI The Journal of Clinical Investigation

Loss of ABCG1 influences regulatory T cell differentiation and atherosclerosis

Hsin-Yuan Cheng, … , Mary Sorci-Thomas, Catherine C. Hedrick

J Clin Invest. 2016;126(9):3236-3246. https://doi.org/10.1172/JCI83136.

Research Article **Inflammation**

ATP-binding cassette transporter G1 (ABCG1) promotes cholesterol accumulation and alters T cell homeostasis, which may contribute to progression of atherosclerosis. Here, we investigated how the selective loss of ABCG1 in T cells impacts atherosclerosis in LDL receptor–deficient (LDLR-deficient) mice, a model of the disease. In LDLR-deficient mice fed a high-cholesterol diet, T cell–specific ABCG1 deficiency protected against atherosclerotic lesions. Furthermore, T cell–specific ABCG1 deficiency led to a 30% increase in Treg percentages in aorta and aorta-draining lymph nodes (LNs) of these mice compared with animals with only LDLR deficiency. When *Abcg1* was selectively deleted in Tregs of LDLR-deficient mice, we observed a 30% increase in Treg percentages in aorta and aorta-draining LNs and reduced atherosclerosis. In the absence of ABCG1, intracellular cholesterol accumulation led to downregulation of the mTOR pathway, which increased the differentiation of naive CD4 T cells into Tregs. The increase in Tregs resulted in reduced T cell activation and increased IL-10 production by T cells. Last, we found that higher ABCG1 expression in Tregs was associated with a higher frequency of these cells in human blood samples. Our study indicates that ABCG1 regulates T cell differentiation into Tregs, highlighting a pathway by which cholesterol accumulation can influence T cell homeostasis in atherosclerosis.

Loss of ABCG1 influences regulatory T cell differentiation and atherosclerosis

Hsin-Yuan Cheng,[1] Dalia E. Gaddis,[1] Runpei Wu,[1] Chantel McSkimming,[2] LaTeira D. Haynes,[1] Angela M. Taylor,[2] Coleen A. McNamara,[2] Mary Sorci-Thomas,[3] and Catherine C. Hedrick[1]

[1]Division of Inflammation Biology, La Jolla Institute for Allergy and Immunology, La Jolla, California, USA. [2]Cardiovascular Research Center and Division of Cardiology, University of Virginia, Charlottesville, Virginia, USA. [3]Department of Medicine, Division of Endocrinology, Medical College of Wisconsin, Milwaukee, Wisconsin, USA.

ATP-binding cassette transporter G1 (ABCG1) promotes cholesterol accumulation and alters T cell homeostasis, which may contribute to progression of atherosclerosis. Here, we investigated how the selective loss of ABCG1 in T cells impacts atherosclerosis in LDL receptor–deficient (LDLR-deficient) mice, a model of the disease. In LDLR-deficient mice fed a high-cholesterol diet, T cell–specific ABCG1 deficiency protected against atherosclerotic lesions. Furthermore, T cell–specific ABCG1 deficiency led to a 30% increase in Treg percentages in aorta and aorta-draining lymph nodes (LNs) of these mice compared with animals with only LDLR deficiency. When *Abcg1* was selectively deleted in Tregs of LDLR-deficient mice, we observed a 30% increase in Treg percentages in aorta and aorta-draining LNs and reduced atherosclerosis. In the absence of ABCG1, intracellular cholesterol accumulation led to downregulation of the mTOR pathway, which increased the differentiation of naive CD4 T cells into Tregs. The increase in Tregs resulted in reduced T cell activation and increased IL-10 production by T cells. Last, we found that higher ABCG1 expression in Tregs was associated with a higher frequency of these cells in human blood samples. Our study indicates that ABCG1 regulates T cell differentiation into Tregs, highlighting a pathway by which cholesterol accumulation can influence T cell homeostasis in atherosclerosis.

Introduction

Atherosclerosis is the main cause of cardiovascular disease and continues to be a leading cause of death worldwide (1, 2). Atherosclerosis is a chronic inflammatory disease that is initiated by the accumulation of cholesterol-containing oxidized LDL in the arterial wall that triggers immune responses. Macrophages and T lymphocytes play major roles in atherosclerosis progression (3). T cell subsets play distinct roles in the development of the disease. Proinflammatory Th1 and Th17 cells are considered driving forces for atherosclerosis, and Tregs are atheroprotective (4–7).

ATP-binding cassette transporter G1 (ABCG1), a member of the ATP-binding cassette transporter family, promotes the efflux of intracellular cholesterol to HDL particles, which transport cholesterol to the liver for excretion (8). ABCG1 is predominantly localized within intracellular compartmental membranes and has been shown to mobilize to the plasma membrane upon cholesterol loading (9). Cholesterol is an essential component of mammalian cell membranes that maintains proper permeability and fluidity of the membrane to ensure normal cell growth and function. Cholesterol has been shown to be involved in cell signaling by assisting the formation of lipid rafts, the specialized microdomains for organizing signaling molecules (10). Intracellular cholesterol homeostasis is maintained by the balance between cholesterol biosynthesis and uptake and its utilization and efflux (11, 12).

ABCG1 is highly expressed in various immune cells including macrophages and T lymphocytes. Bensinger et al. illustrated an important role for ABCG1 in T cell proliferation (13), and our group also reported that ABCG1-deficient CD4$^+$ T cells showed enhanced T cell receptor signaling due to altered lipid raft formation (14). The development and function of NKT cells is also affected by the absence of ABCG1 in a cell-intrinsic manner (15). Collectively, these data illustrate that ABCG1 plays an important role in T cell homeostasis and function that may impact atherosclerosis progression. Our goal in this study was to test whether the absence of ABCG1 selectively in T cells alters the development of atherosclerosis.

Results

T cell–specific deletion of Abcg1 leads to an increase in Tregs. To test the function of *Abcg1* in T cells, we generated conditional KO mice in which *Abcg1* was selectively deleted in T cells using *Lck-Cre*. Mice with 2 loxP sites flanking the Walker domain of exon 3 of *Abcg1* were bred with the *Lck-Cre* mouse line (16). *Lck* promoter–driven *Cre* expression deletes *Abcg1* gene expression early at the double-negative (DN) stage of thymocyte development and therefore selectively eliminates *Abcg1* expression in all T cell receptor β$^+$ (TCRβ$^+$) T cells (17). The complete deletion of *Abcg1* in CD4$^+$ T cells in thymus and spleen of *Lck-Cre*$^+$ *Abcg1*$^{fl/fl}$ mice was confirmed by Western immunoblotting (Figure 1A). In contrast, ABCG1 expression remained normal in the *Lck-Cre*$^-$ *Abcg1*$^{fl/fl}$ littermate mice (Figure 1A). *Abcg1* global KO mice and WT C57BL/6J mice were used as positive and negative controls, respectively (Figure 1A). Having confirmed successful *Abcg1* deletion in T cells using *Lck-Cre* mice, we analyzed the T cell compartment in peripheral lymph nodes

Authorship note: H.Y. Cheng and D.E. Gaddis contributed equally to this work.
Conflict of Interest: The authors have declared that no conflict of interest exists.
Submitted: June 5, 2015; **Accepted:** June 2, 2016.
Reference information: *J Clin Invest*. 2016;126(9):3236–3246. doi:10.1172/JCI83136.

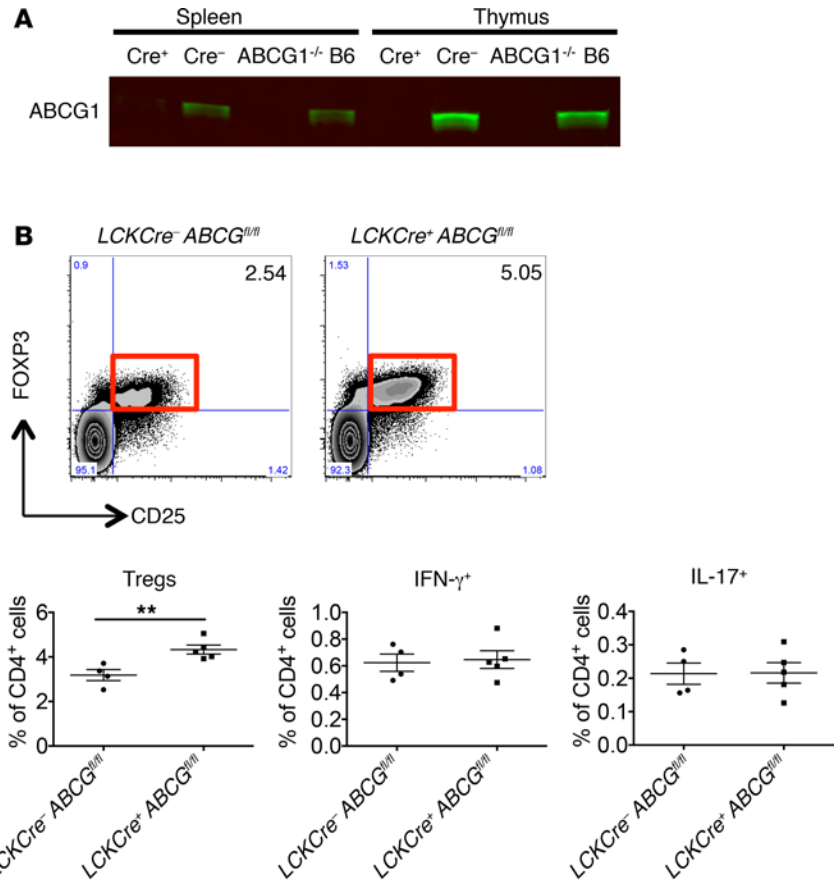

Figure 1. Tregs are increased in mice with T cell–specific deficiency of ABCG1. (**A**) ABCG1 protein expression was completely absent in T cells isolated from spleen and thymus of *Lck-Cre*$^{+}$ *Abcg1*$^{fl/fl}$ mice (*Cre*$^{+}$). T cells from *Lck-Cre*$^{-}$ *Abcg1*$^{fl/fl}$ (*Cre*$^{-}$) littermate controls expressed normal levels of ABCG1. T cells from mice with a systemic deficiency of ABCG1 (*Abcg1*$^{-/-}$) and WT C57BL/6 mice served as negative and positive controls, respectively. Each lane represents a pool of 3 mice. (**B**) Treg levels were elevated in the peripheral LNs of Cre^{+} mice. Top panel: Representative FACS plots of CD4^{+}CD25^{+}FOXP3^{+} Tregs in Cre^{-} and Cre^{+} mice. Bottom panel: Percentages of Tregs and IFN-γ– and IL-17–producing Teffs in the peripheral LNs of Cre^{-} and Cre^{+} mice. Data were averaged from 4 to 5 mice per group and are presented as individual mice. $^{**}P < 0.01$, by unpaired Student's *t* test to determine differences between 2 groups.

(LNs) of *Lck-Cre*$^{-}$ *Abcg1*$^{fl/fl}$ and *Lck-Cre*$^{+}$ *Abcg1*$^{fl/fl}$ mice fed a chow diet. We found a significant 30%–40% increase in Tregs in peripheral LNs (Figure 1B), with no changes in IFN-γ– or IL-17–producing effector T cells. Analysis of the thymus also showed a significant increase in Treg production in thymus of *Lck-Cre*$^{+}$ *Abcg1*$^{fl/fl}$ mice compared with that observed in littermate *Lck-Cre*$^{-}$ *Abcg1*$^{fl/fl}$ mice (Supplemental Figure 1A), whereas the numbers of thymic CD4, CD8, and double-positive (DP) CD4^{+}CD8^{+} precursors did not change (Supplemental Figure 1B). This was accompanied by an increase in the intracellular expression of FOXP3, the master transcription regulator of Tregs in thymic Tregs of *Lck-Cre*$^{+}$ *Abcg1*$^{fl/fl}$ mice (Supplemental Figure 1C).

To determine whether the increase in Tregs was due to a cell-intrinsic developmental advantage caused by the absence of ABCG1, we used a mixed chimera approach to study Tregs in the same recipient mice (15). In order to distinguish the origin of the Tregs, mice used as donors expressed CD45.1 (WT) or CD45.2 (*Lck-Cre*$^{+}$ *Abcg1*$^{fl/fl}$) alleles, respectively. Bone marrow cells from WT CD45.1 mice and *Lck-Cre*$^{+}$ *Abcg1*$^{fl/fl}$ mice were mixed at a 1:1 ratio and injected into irradiated CD45.1/2 WT recipient mice. After 10 weeks of reconstitution, spleens were harvested for flow cytometric analysis. The flow cytometric gating strategy for donor Tregs is shown in Figure 2A. The majority of Tregs in the recipient mice expressed the CD45.2 allele, indicating that these FOXP3^{+}CD25^{+} Tregs were of *Lck-Cre*$^{+}$ *Abcg1*$^{fl/fl}$ origin (76.0% ± 2.7% of CD45.2 vs. 12.9% ± 2.4% of CD45.1, $P < 0.0001$) (Figure 2A).

These data suggest a developmental advantage for T cells lacking ABCG1. To follow up, we performed an ex vivo assay to assess the propensity of naive T cells lacking ABCG1 to differentiate into Tregs. Naive T cells from *Lck-Cre*$^{-}$ *Abcg1*$^{fl/fl}$ and *Lck-Cre*$^{+}$ *Abcg1*$^{fl/fl}$ mice were cultured with anti-CD3/CD28 Abs in the presence of TGF-β for 72 hours to skew the cells toward a Treg lineage. We found an increase of approximately 30% in the ability of naive T cells lacking ABCG1 to differentiate into Tregs (Figure 2B). We also performed an in vivo Treg differentiation experiment using adoptive transfer. Naive CD4^{+} cells from WT mice (on a CD45.1 background) and *Lck-Cre*$^{+}$ *Abcg1*$^{fl/fl}$ mice (on a CD45.2 background) were injected at a 1:1 ratio into immunodeficient *Rag1*$^{-/-}$ mice (on a CD45.1/2 background). *Rag1*$^{-/-}$ mice possess no T or B cells (18), so any Tregs appearing in the mice after reconstitution are derived from donor cells. After a 10-day reconstitution, the majority of Tregs in the peripheral LNs of *Rag1*$^{-/-}$ mice expressed the CD45.2 allele, indicating that these Tregs were derived from *Lck-Cre*$^{+}$ *Abcg1*$^{fl/fl}$ naive cells that lacked ABCG1 (Figure 2C). Hence, *Lck-Cre*$^{+}$ *Abcg1*$^{fl/fl}$ naive T cells displayed a preferential differentiation into Tregs in vivo. Finally, we analyzed proliferation and apoptosis rates of Tregs in these mice. For proliferation, mice were injected with BrdU, and BrdU incorporation into Tregs from peripheral LNs was examined 3 days after injection as a measure of proliferation. We observed no differences in BrdU incorporation, showing that the proliferation of ABCG1-deficient Tregs and WT Tregs was similar (Supplemental Figure 2). We observed similar results when we examined the percentages of Ki67^{+} cells in Tregs (Supplemental Figure 2). Next, we examined Treg apoptosis in peripheral LNs using annexin V and caspase-3 staining and observed no differences between groups, suggesting that there were no major differences in apoptosis in the Tregs lacking ABCG1 (Supplemental Figure 3).

We next evaluated the suppressive activity of Tregs from *Lck-Cre*$^{-}$ *Abcg1*$^{fl/fl}$ and *Lck-Cre*$^{+}$ *Abcg1*$^{fl/fl}$ mice. The ability of Tregs to suppress the proliferation of cocultured T effector cells (Teffs) is commonly used as an indicator of Treg function (19). CD4^{+}CD62L^{+}CD44^{-} naive

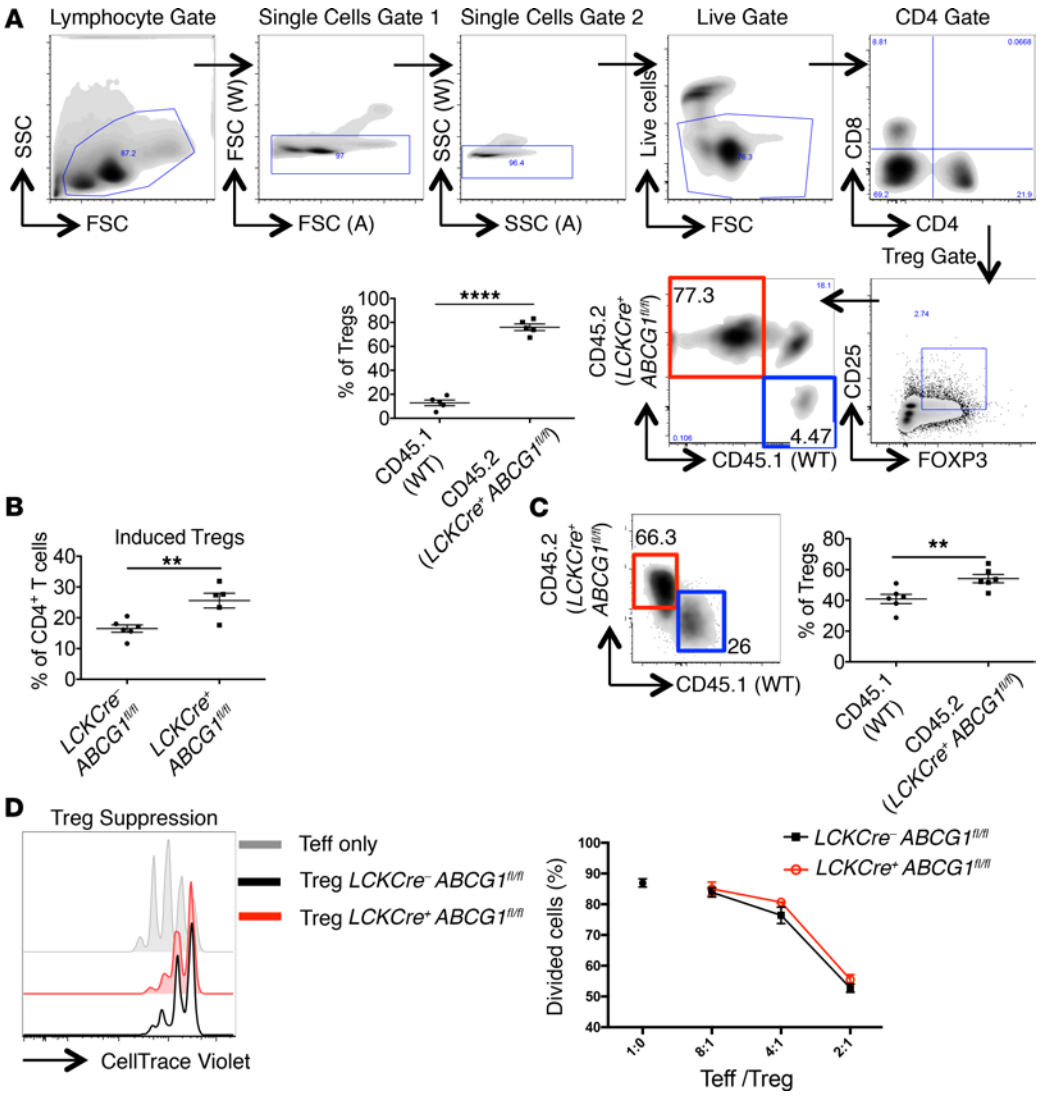

Figure 2. The advantage of *Lck-Cre*⁺ *Abcg1*$^{fl/fl}$ Treg development is intrinsic. (**A**) CD45.1 (WT) and CD45.2 (*Lck-Cre*⁺ *Abcg1*$^{fl/fl}$) bone marrow cells were injected at a 1:1 ratio into irradiated CD45.1/2 heterozygous recipient mice, which were analyzed 10 weeks later. Gating strategy shows the splenic CD45.1/CD45.2 Treg composition. Representative FACS plot shows CD45.1 (blue box) versus CD45.2 (red box) Tregs. Graph shows the percentages of CD45.1⁺ (WT) and CD45.2⁺ (*Lck-Cre*⁺ *Abcg1*$^{fl/fl}$) Tregs in recipient mice. *N* = 5 mice per group. FSC, forward scatter; SSC, side scatter; W, width. (**B** and **C**) Increased Treg differentiation from naive *Lck-Cre*⁺ *Abcg1*$^{fl/fl}$ CD4⁺ cells. (**B**) Naive CD4⁺ T cells from *Lck-Cre*⁺ *Abcg1*$^{fl/fl}$ mice and *Lck-Cre*⁻ *Abcg1*$^{fl/fl}$ littermates were cultured with CD3/CD28 Abs plus TGF-β for 72 hours. *N* = 5–6 mice per group. (**C**) Naive CD4⁺ T cells isolated from WT (CD45.1) and *Lck-Cre*⁺ *Abcg1*$^{fl/fl}$ (CD45.2) donor mice were transferred into *Rag1*$^{-/-}$ recipient mice at a 1:1 ratio, and 10 days later, the recipients' peripheral LNs were analyzed. Representative FACS plot shows CD45.1 (WT; blue box) versus CD45.2 (*Lck-Cre*⁺ *Abcg1*$^{fl/fl}$; red box) Tregs. Dot plot shows the percentages of WT- and *Lck-Cre*⁺ *Abcg1*$^{fl/fl}$–expressing Tregs in the recipient mice. *N* = 5–6 mice per group. (**D**) An in vitro suppression assay was performed. CellTrace Violet–labeled WT naive CD4⁺CD25⁻CD62L⁺CD44⁻ T cells (Teff) were cocultured with or without CD4⁺CD25⁺ Tregs from *Lck-Cre*⁻ *Abcg1*$^{fl/fl}$ and *Lck-Cre*⁺ *Abcg1*$^{fl/fl}$ mice at a Teff/Treg ratio of 2:1. Representative plots of Teff cell division are shown. Graph shows the percentages of CellTrace Violet–diluted Teff cells (divided cell percentage) at an increasing Teff/Treg ratio. Results were averaged from 4 to 6 mice per group. $^{**}P < 0.01$ and $^{****}P < 0.0001$, by unpaired Student's *t* test to determine differences between 2 groups.

Teffs from CD45.1 WT mice were cocultured with Tregs from either *Lck-Cre*⁻ *Abcg1*$^{fl/fl}$ or *Lck-Cre*⁺ *Abcg1*$^{fl/fl}$ mice, and the ability of Tregs to suppress the proliferation of Teff cells was measured following stimulation with α-CD3. We found that the suppressive activities of *Lck-Cre*⁻ *Abcg1*$^{fl/fl}$ and *Lck-Cre*⁺ *Abcg1*$^{fl/fl}$ Tregs were similar (Figure 2D). Taken together, these results indicate that ABCG1 deficiency in T cells causes a cell-intrinsic preference of naive CD4⁺ T cell differentiation into atheroprotective Tregs. Thus, mice lacking ABCG1 expression in T cells develop higher numbers of Tregs in vivo, although the suppressive activity of the Tregs does not change.

ABCG1 deficiency selectively in T cells protects mice against atherosclerosis. We next examined the impact of T cell–selective deletion of *Abcg1* on atherosclerosis development. To facilitate this, we bred *Lck-Cre*⁺ *Abcg1*$^{fl/fl}$ mice onto the atherosclerosis-susceptible *Ldlr*$^{-/-}$ background. *Lck-Cre*⁺ *Abcg1*$^{fl/fl}$ *Ldlr*$^{-/-}$ mice and their *Lck-Cre*⁻ *Abcg1*$^{fl/fl}$ *Ldlr*$^{-/-}$ littermates were fed a high-cholesterol diet (1.25% cholesterol, 40 cal% fat) for 15 weeks (20). Plasma cholesterol and triglyceride levels were similar between the 2 groups, suggesting that the absence of ABCG1 in T cells alone does not contribute to a global change in plasma lipid profiles (Supplemental Figure 4).

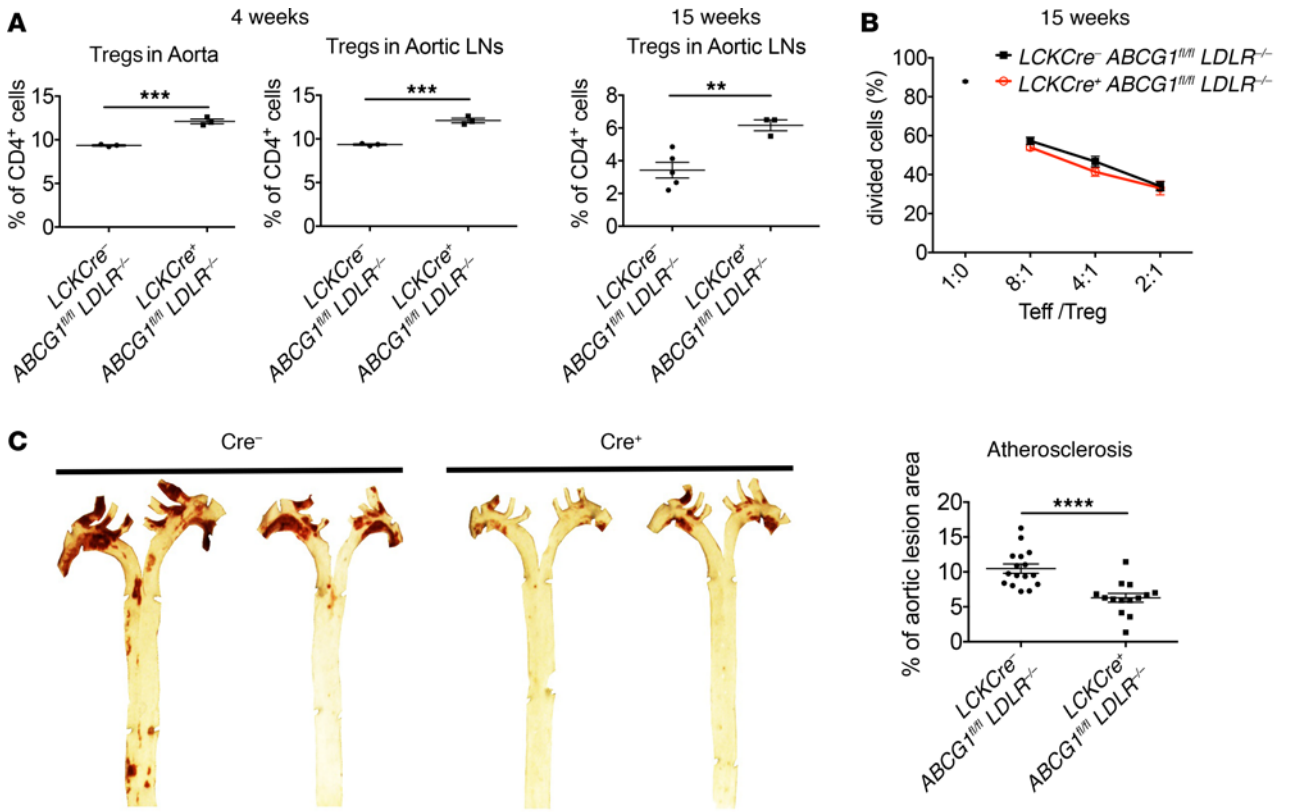

Figure 3. Mice with T cell–specific deletion of ABCG1 are protected against atherosclerosis. (**A**) *Lck-Cre*$^{+}$ *Abcg1*$^{fl/fl}$ *Ldlr*$^{-/-}$ and *Lck-Cre*$^{-}$ *Abcg1*$^{fl/fl}$ *Ldlr*$^{-/-}$ littermates were fed a high-cholesterol diet for either 4 or 15 weeks, and the percentages of Tregs were determined in the aorta and aortic LNs. Each dot represents an individual mouse. *N* = 4–5 mice per group. (**B**) In vitro suppression assay performed with Tregs from mice on an *Ldlr*$^{-/-}$ background and fed a high-cholesterol diet for 15 weeks. Results showed no change in Treg-suppressive activity in the absence of ABCG1. Data were averaged from 4 mice per group. (**C**) Atherosclerotic lesion area in aorta after 15 weeks of high-cholesterol diet feeding was analyzed in *Lck-Cre*$^{+}$ *Abcg1*$^{fl/fl}$ *Ldlr*$^{-/-}$ mice and *Lck-Cre*$^{-}$ *Abcg1*$^{fl/fl}$ *Ldlr*$^{-/-}$ littermates. Representative oil red O staining (red) in the aortic arches of *Lck-Cre*$^{+}$ *Abcg1*$^{fl/fl}$ *Ldlr*$^{-/-}$ (Cre^{+}) mice and *Lck-Cre*$^{-}$ *Abcg1*$^{fl/fl}$ *Ldlr*$^{-/-}$ (Cre^{-}) littermates. Graph shows the quantification of lesion area as a percentage of aortic surface area in matched Cre^{+} and Cre^{-} mice after 15 weeks of high-cholesterol diet feeding. Results are shown for individual mice. *N* = 14–16 mice per group. $^{**}P < 0.01$, $^{***}P < 0.001$, and $^{****}P < 0.0001$, by unpaired Student's *t* test to determine differences between 2 groups.

Treg frequencies were increased by approximately 30% in aorta and para-aortic LNs at both 4 weeks and 15 weeks after high-cholesterol diet feeding (Figure 3A), although Treg numbers in both control and Cre^{+} mice decreased over time. This is consistent with studies by Lichtman and colleagues (21), who showed that Treg numbers decrease in aorta during atherosclerosis progression. Again, the suppressive activities of *Lck-Cre*$^{-}$ *Abcg1*$^{fl/fl}$ *Ldlr*$^{-/-}$ and *Lck-Cre*$^{+}$ *Abcg1*$^{fl/fl}$ *Ldlr*$^{-/-}$ Tregs were not different when the mice were fed a high-cholesterol diet for 15 weeks (Figure 3B). The atherosclerotic lesion area in *Lck-Cre*$^{+}$ *Abcg1*$^{fl/fl}$ *Ldlr*$^{-/-}$ and *Lck-Cre*$^{-}$ *Abcg1*$^{fl/fl}$ *Ldlr*$^{-/-}$ littermates after 15 weeks of high-cholesterol diet feeding was quantified in the aorta using en face analysis (22). A 40% reduction of atherosclerotic lesion area was found in aorta of *Lck-Cre*$^{+}$ *Abcg1*$^{fl/fl}$ *Ldlr*$^{-/-}$ mice compared with that found in aorta of *Lck-Cre*$^{-}$ *Abcg1*$^{fl/fl}$ *Ldlr*$^{-/-}$ littermates (6.3% ± 0.6% in *Lck-Cre*$^{+}$ *Abcg1*$^{fl/fl}$ *Ldlr*$^{-/-}$ mice vs. 10.5% ± 0.7% in *Lck-Cre*$^{-}$ *Abcg1*$^{fl/fl}$ *Ldlr*$^{-/-}$ mice, $P < 0.0001$) (Figure 3C). Since Tregs have been shown by others to be atheroprotective (23, 24), we hypothesized that the decreased atherosclerosis observed in *Lck-Cre*$^{+}$ *Abcg1*$^{fl/fl}$ *Ldlr*$^{-/-}$ mice was due to the increased number of Tregs.

As Tregs function to suppress Teff cell activation, we examined the activation state of CD4^{+} Teff cells in the aorta in mice fed a high-cholesterol diet for 15 weeks. We found that *Lck-Cre*$^{+}$ *Abcg1*$^{fl/fl}$ *Ldlr*$^{-/-}$ mice had a 50% reduction in the number of activated CD44^{+}CD62L^{-}CD4^{+} T cells in the aorta (Figure 4A). Moreover, CD4^{+} T cells in the para-aortic LNs had increased expression of programmed death-1 (PD-1) (Figure 4B) and increased surface expression of TCRβ (Figure 4C), further illustrating reduced T cell activation. Taken together, these results indicate that the increase in Treg numbers in the absence of ABCG1 functionally suppresses Teff cell activation in the aorta and supports the notion that the reduced atherosclerosis seen in these mice is caused by enhanced Treg function.

Absence of ABCG1 selectively in FOXP3^{+} *Tregs is atheroprotective.* We next crossed our *Abcg1*$^{fl/fl}$ *Ldlr*$^{-/-}$ mice with *Foxp3-Cre* mice. FOXP3 is the master transcriptional regulator of Tregs and is selectively expressed in Tregs (25). The resulting *Foxp3-Cre*$^{+}$ *Abcg1*$^{fl/fl}$ *Ldlr*$^{-/-}$ mice showed no *Abcg1* mRNA expression in sorted Tregs from blood, indicating complete deletion of *Abcg1* in Tregs by *Foxp3-Cre* expression (Figure 5A). We asked whether the absence of ABCG1 selectively in Tregs alone would provide atheroprotection. When fed a high-cholesterol diet for 15 weeks, the *Foxp3-Cre*$^{+}$ *Abcg1*$^{fl/fl}$ *Ldlr*$^{-/-}$ mice showed a reduction of approximately 50% in atherosclerotic lesion area in aorta compared with that observed

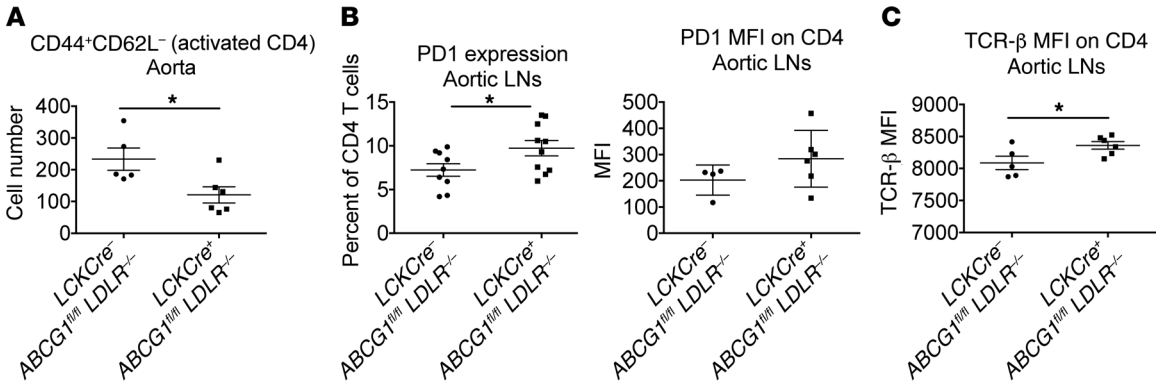

Figure 4. T cells from mice with T cell–specific deletion of ABCG1 show increased PD-1 expression and decreased activation during atherosclerosis development. *Lck-Cre*$^+$ *Abcg1*$^{fl/fl}$ (Cre$^+$) mice and *Lck-Cre*$^-$ *Abcg1*$^{fl/fl}$ (Cre$^-$) littermates on an *Ldlr*$^{-/-}$ background were fed a high-cholesterol diet (1.25% cholesterol) for 15 weeks, and the percentages of activated (CD44$^+$CD62L$^-$) CD4 T cells (**A**), the percentages and MFI of PD-1 expression on CD4$^+$ T cells (**B**), and the MFI of TCRβ (**C**) were determined in cells obtained from either the aorta or aortic LNs. Results are shown for individual mice. N = 4–10 mice per group. *$P < 0.05$, by unpaired Student's t test to determine differences between 2 groups.

in control mice (8.0% ± 0.5% vs. 16.5% ± 0.8%, $P < 0.0001$) (Figure 5B). This is consistent with the atherosclerosis data in our *Lck-Cre*$^+$ *Abcg1*$^{fl/fl}$ *Ldlr*$^{-/-}$ model, and such data indicate that loss of ABCG1 in Tregs alone is sufficient to exert a significant atheroprotective effect in vivo. Treg percentages in the para-aortic LNs were significantly higher in the high-cholesterol diet–fed *Foxp3-Cre*$^+$ *Abcg1*$^{fl/fl}$ *Ldlr*$^{-/-}$ mice (Figure 5C). Furthermore, there were greater numbers of IL-10$^+$CD4$^+$ T cells (Figure 5D) and fewer IL-17$^+$CD4$^+$ T cells (Figure 5E) present in the para-aortic LNs of *Foxp3-Cre*$^+$ *Abcg1*$^{fl/fl}$ *Ldlr*$^{-/-}$ mice compared with the littermate control mice fed a high-cholesterol diet, suggesting a phenotypic skewing of Teffs to an antiinflammatory phenotype in the presence of increased numbers of Tregs.

Increased cholesterol accumulation and inhibition of mTOR signaling in Tregs in the absence of ABCG1. The development of Tregs and Teffs requires different metabolic checkpoints. mTOR activity is associated with the differential regulation of T cell subsets. For example, the differentiation of Th1, Th2, and Th17 Teffs requires high mTOR activation, while Treg differentiation shows the opposite (26, 27). Proper cholesterol trafficking in cells has been shown to be critically important for mTOR activation, as blockage of cholesterol trafficking through lysosomes results in an inhibition of mTOR activity (28). ABCG1 functions to transport cholesterol from cells to HDL particles, as well as to maintain intracellular cholesterol homeostasis (8, 9, 29, 30). Fluorescent filipin binds specifically to cholesterol (31) and was used to measure the cholesterol content of freshly isolated Tregs from *Lck-Cre*$^+$ *Abcg1*$^{fl/fl}$ *Ldlr*$^{-/-}$ mice fed a high-cholesterol diet. We found a significantly higher filipin content (by median fluorescence intensity [MFI]) in *Lck-Cre*$^+$ *Abcg1*$^{fl/fl}$ *Ldlr*$^{-/-}$ Tregs (Figure 6A) compared with that observed in Tregs from littermate controls, which indicates an accumulation of cholesterol in these cells. Inhibition of mTOR triggers the phosphorylation and activation of STAT5, which is directly and positively associated with Treg development and homeostasis. STAT5 phosphorylation and activation are critical for the induction and maintenance of FOXP3 expression (32, 33). To investigate whether mTOR and STAT5 signaling were affected, Tregs from peripheral LNs of *Lck-Cre*$^-$ *Abcg1*$^{fl/fl}$ *Ldlr*$^{-/-}$ and *Lck-Cre*$^+$ *Abcg1*$^{fl/fl}$ *Ldlr*$^{-/-}$ mice were stimulated with IL-2 (34), and phosphorylation of both ribosomal protein S6 kinase (S6, a downstream target of mTOR) and STAT5 were measured by flow cytometry (35). We found a significant decrease in S6 kinase phosphorylation in *Lck-Cre*$^+$ *Abcg1*$^{fl/fl}$ *Ldlr*$^{-/-}$ Tregs in response to IL-2 stimulation, which is indicative of reduced mTOR activation (Figure 6B). Concomitantly, we observed an increase in STAT5 phosphorylation in *Lck-Cre*$^+$ *Abcg1*$^{fl/fl}$ *Ldlr*$^{-/-}$ Tregs, which is in accordance with previous studies showing that inhibition of mTOR led to enhanced STAT5 signaling (34) (Figure 6C). We repeated this in *Foxp3-Cre*$^+$ *Abcg1*$^{fl/fl}$ *Ldlr*$^{-/-}$ Tregs isolated from mice fed a high-cholesterol diet for 15 weeks. Again, we saw increased cholesterol content in isolated Tregs as measured by filipin (Figure 6D) and an increase in lipid raft content as measured by cholera toxin-B staining (Figure 6E). Finally, we also found a decrease in S6 kinase phosphorylation in *Foxp3-Cre*$^+$ *Abcg1*$^{fl/fl}$ *Ldlr*$^{-/-}$ Tregs (Figure 6F), similar to what we observed in *Lck-Cre*$^+$ *Abcg1*$^{fl/fl}$ *Ldlr*$^{-/-}$ Tregs (Figure 6B). Our data suggest that an increase in intracellular cholesterol due to the absence of ABCG1 in Tregs leads to mTOR inhibition and subsequent STAT5 activation, which in turn favors Treg development.

Association between ABCG1 and blood Treg levels in humans. Overall, our data indicate that an absence of ABCG1 in T cells induces Treg differentiation in mice. Importantly, we wanted to determine whether there is a similar inverse association between ABCG1 levels and Tregs in human blood. Human blood samples were obtained from patients undergoing medically necessary cardiac catheterization at the University of Virginia. Information on the human subjects participated in our study is shown in Table 1. Treg percentages in blood were quantified by flow cytometry (identified as CD4$^+$CD25$^+$CD127$^-$FOXP3$^+$ cells). We also sorted CD4$^+$CD25^{hi} Tregs from part of the human blood sample for RNA analysis. RNA was isolated from the sorted Tregs, and *ABCG1* mRNA expression was measured. In agreement with our conditional KO mouse data, we observed a significant negative correlation ($P < 0.03$) between ABCG1 expression levels in Tregs and the percentages of Tregs present in human blood (Figure 7). Taken together, the mouse and human studies indicate that ABCG1 plays an important role in Treg differentiation.

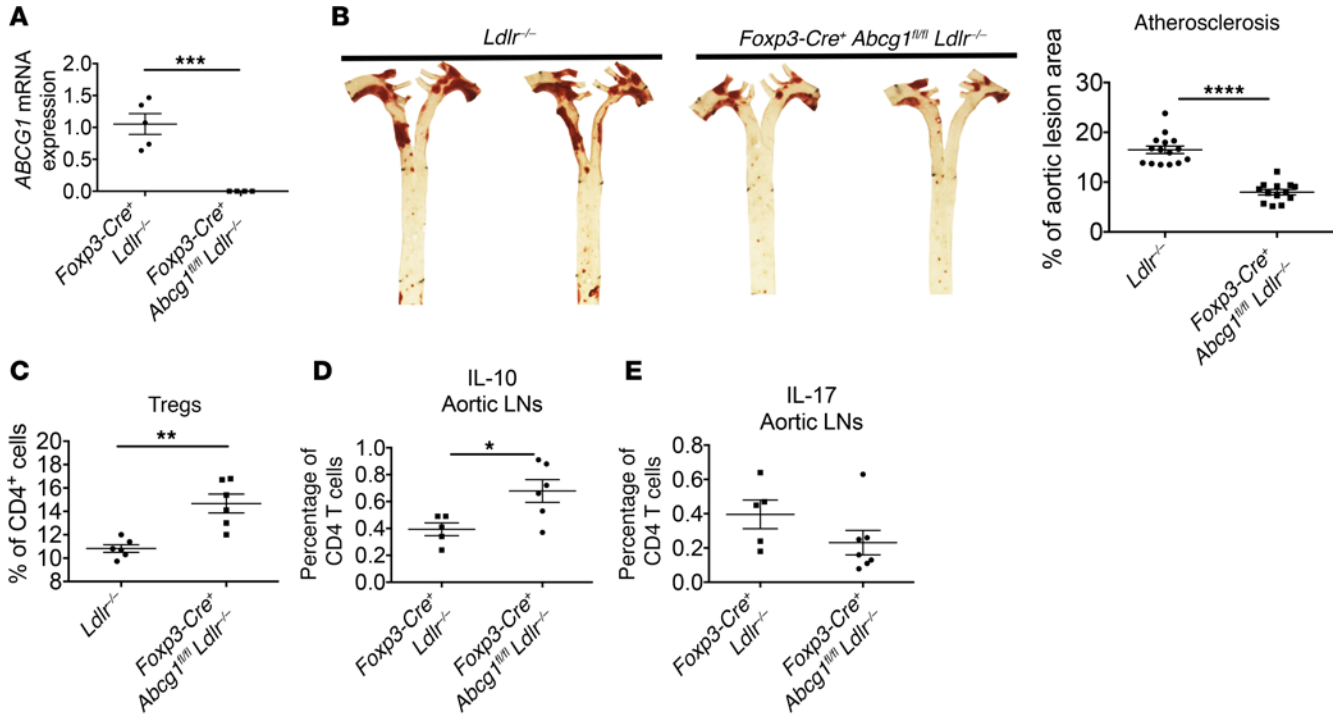

Figure 5. Mice with FOXP3-specific deficiency of ABCG1 show decreased atherosclerosis and an increase in Tregs and IL-10. (**A**) Expression of *Abcg1* mRNA was undetectable in Tregs sorted from the blood of *Foxp3-Cre*$^{+}$ *Abcg1*$^{fl/fl}$ *Ldlr*$^{-/-}$ mice. Results are shown for individual mice. N = 4–5 mice per group. (**B**–**C**) *Foxp3-Cre*$^{+}$ *Abcg1*$^{fl/fl}$ *Ldlr*$^{-/-}$ and *Ldlr*$^{-/-}$ control mice were fed a high-cholesterol diet for 15 weeks, and the atherosclerotic lesion area in aortae (**B**) and Treg percentages in the aortic LNs (**C**) were analyzed. (**B**) Representative oil red O staining (red) in the aortic arches of *Ldlr*$^{-/-}$ and *Foxp3-Cre*$^{+}$ *Abcg1*$^{fl/fl}$ *Ldlr*$^{-/-}$ mice. Graph shows the quantification of the lesion area as a percentage of aortic surface area in matched *Ldlr*$^{-/-}$ control and *Foxp3-Cre*$^{+}$ *Abcg1*$^{fl/fl}$ *Ldlr*$^{-/-}$ mice after 15 weeks of high-cholesterol diet feeding. Results are shown for individual mice. N = 13–15 (**B**) or 6 (**C**) mice per group. (**D**–**E**) *Foxp3-Cre*$^{+}$ *Abcg1*$^{fl/fl}$ *Ldlr*$^{-/-}$ mice and *Foxp3-Cre*$^{+}$ *Ldlr*$^{-/-}$ controls were fed a high-cholesterol diet for 15 weeks, and the capacity of CD4 T cells to produce IL-10 (**D**) and IL-17 (**E**) was determined in aortic LNs following 4 hours of stimulation with PMA and ionomycin. Data shown represent individual mice. N = 5–7 mice per group. *P < 0.05, **P < 0.01, ***P < 0.001, and ****P < 0.0001, by unpaired Student's t test to determine differences between 2 groups.

Discussion

Atherosclerosis is an inflammatory disease driven mainly by macrophages and T cells (3). ABCG1 is a cholesterol transporter that is involved in cellular cholesterol homeostasis. The role of ABCG1 in macrophages and how it affects atherosclerosis has been studied extensively (30, 36). ABCG1 has been shown by Bensinger et al. and our group to regulate the intracellular cholesterol content of T cells (13, 14). However, the function of ABCG1 in CD4^{+} T cell subsets in atherosclerosis has not been studied, and in this report, we show that ABCG1 influences the development of atherosclerosis by affecting Treg development. The use of *Lck-Cre*$^{+}$ *Abcg1*$^{fl/fl}$ mice allowed us to specifically study the function of ABCG1 in T cells, and the use of *Foxp3-Cre*$^{+}$ *Abcg1*$^{fl/fl}$ mice allowed us to study the function of ABCG1 selectively in Tregs. Using both *Lck-Cre*$^{+}$ *Abcg1*$^{fl/fl}$ and *Foxp3-Cre*$^{+}$ *Abcg1*$^{fl/fl}$ mice, we found that the CD4^{+}CD25^{+}FOXP3^{+} Treg subset, but not other Teff subsets, was specifically increased in the absence of ABCG1. This increase in Treg numbers was cell intrinsic, as there was an increased propensity for naive CD4^{+} T cells to differentiate into Tregs, which was probably due to inhibition of mTOR signaling by the accumulation of cholesterol and increased lipid rafts that occurs in the absence of ABCG1.

T cell–specific ABCG1-deficient mice on an *Ldlr*$^{-/-}$ background had a 40% reduction in atherosclerotic lesion size when fed a high-cholesterol diet compared with that observed in their *Abcg1*$^{+/+}$ littermates. Since Tregs are known to be antiatherogenic, we reasoned that the decrease in atherosclerosis development in *Lck-Cre*$^{+}$ *Abcg1*$^{fl/fl}$ *Ldlr*$^{-/-}$ mice was due to the observed increase in Tregs in these mice. Furthermore, a similar reduction in atherosclerotic lesion size in *Ldlr*$^{-/-}$ mice with Treg-specific *Abcg1* deletion, using *Foxp3-Cre* to drive gene deletion, indicated that the absence of ABCG1 in Tregs alone is sufficient to drive atheroprotection. A key point in these studies is that the suppressive activity of individual Tregs did not change, but overall, we found an increased number of Tregs in vivo. As a result of this Treg increase, CD4 Teffs were less activated and were skewed to produce IL-10, which is atheroprotective (37–40). Thus, the increased number of suppressive Tregs functionally inhibited Teff activation in vivo.

Previously, we observed changes in CD4^{+} T cell proliferation in the global *Abcg1*$^{-/-}$ mice (14), yet we did not observe these changes in the *Lck-Cre*$^{+}$ *Abcg1*$^{fl/fl}$ mice. In our previous work using *Abcg1* whole-body KO mice, CD4^{+} T cells from these global ABCG1-deficient mice proliferated more readily when adoptively transferred into *Rag1*$^{-/-}$ recipients, suggesting a cell-intrinsic function

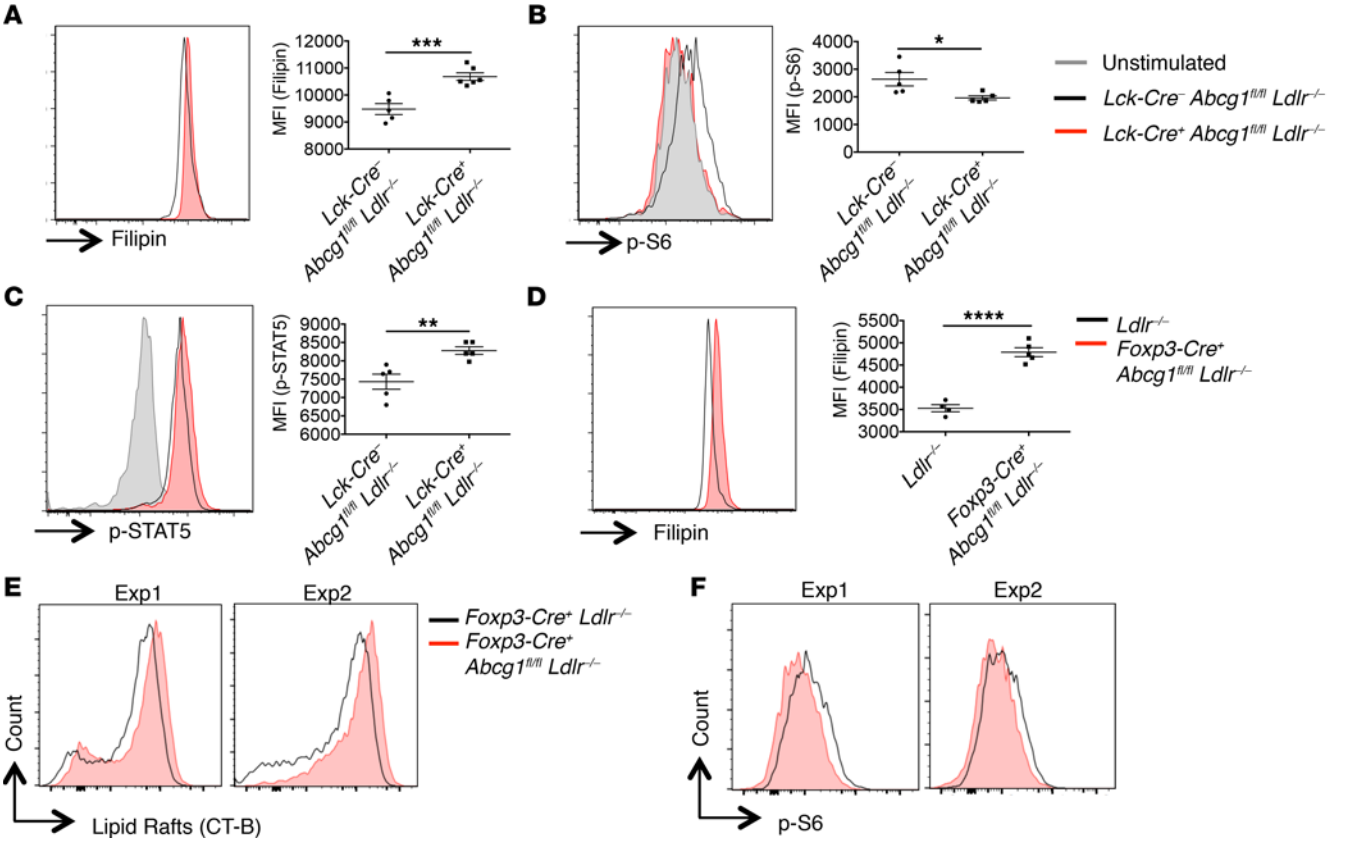

Figure 6. Absence of ABCG1 results in increased cellular cholesterol and lipid rafts, inhibition of mTOR signaling, and increased p-STAT5 signaling. (**A**–**C**) Cholesterol content using filipin staining (**A**) p-S6 (**B**) and p-STAT5 (**C**) in *Lck-Cre*$^{+}$ *Abcg1*$^{fl/fl}$ *Ldlr*$^{-/-}$ Tregs compared with Tregs from *Lck-Cre*$^{-}$ *Abcg1*$^{fl/fl}$ *Ldlr*$^{-/-}$ littermates. Cells were isolated from aortic LNs in **A**–**C** and were stimulated with 100 U/ml IL-2 for 15 minutes in **B** and **C**. Red line indicates *Lck-Cre*$^{+}$ *Abcg1*$^{fl/fl}$ *Ldlr*$^{-/-}$ Tregs; black line indicates *Lck-Cre*$^{-}$ *Abcg1*$^{fl/fl}$ *Ldlr*$^{-/-}$ Tregs. An unstimulated sample is shown in gray in **B** and **C**. Results are shown for individual mice. *N* = 5–6 mice per group. (**D**) Filipin staining showed an increase in intracellular cholesterol in Tregs in aortic LNs from *Foxp3-Cre*$^{+}$ *Abcg1*$^{fl/fl}$ *Ldlr*$^{-/-}$ mice (red) compared with *Ldlr*$^{-/-}$ control mice (black) following 15 weeks of high-cholesterol diet feeding. Results are shown for individual mice. *N* = 4–5 mice per group. (**E**–**F**) *Foxp3-Cre*$^{+}$ *Abcg1*$^{fl/fl}$ *Ldlr*$^{-/-}$ and *Foxp3-Cre*$^{+}$ *Ldlr*$^{-/-}$ control mice were fed a high-cholesterol diet for 15 weeks, and lipid rafts and p-S6 were measured in Tregs in the aortic LNs. Plots represent 2 separate experiments (Exp1 and Exp2). **P* < 0.05, ***P* < 0.01, ****P* < 0.001, and *****P* < 0.0001, by unpaired Student's *t* test to determine differences between 2 groups.

for ABCG1 in regulating T cell proliferation. It is possible that there is a small amount of ABCG1 functionally present in the conditional KO mice that is undetectable by immunoblotting, as it is often quite difficult to obtain 100% deletion using the *Cre-loxp* system. Or, it is possible that there are additional metabolic changes in the CD4^{+} T cells in the global KO mouse that are not found in the CD4^{+} T cells in conditional KO mice. Alternatively, cholesterol accumulation in ABCG1 deficiency probably operates at more than one stage of T cell development.

This work and the work of others indicate that proteins that influence the structural order and composition of lipid rafts significantly impact TCR signaling and hence T cell differentiation and activation (13, 41–43). ABCG1 facilitates the transport of cholesterol and 7-ketocholesterol from the plasma membrane to HDL in the process of reverse cholesterol transport (44, 45). Although the focus of this study is on ABCG1, other proteins that regulate the cholesterol content of the cell or the lipid raft content are also likely to regulate Treg function. Examples include SREBP, liver X receptor (LXR), Niemann-Pick type C (NPC1 and NPC2), ABCA1, and apolipoprotein A-I (APOA-I). Bensinger et al. have shown that LXRs, particularly LXRβ, are important regulators of lymphocyte membrane cholesterol content and cell proliferation (13). LXRs regulate the expression of both *ABCG1* and *ABCA1* in cells, including lymphocytes (13, 46). Although ABCG1 seems to play a more critical role than ABCA1 in regulating T cell proliferation in response to membrane sterol content (13), ABCA1 probably also plays a role in the maintenance of Treg function, as it is expressed in Tregs (41). In support of this, ABCA1 effluxes cholesterol from plasma membranes to APOA-I in reverse cholesterol transport, also regulating plasma membrane cholesterol content. Mice lacking both APOA-I and the LDL receptor (*Apoa1*$^{-/-}$ *Ldlr*$^{-/-}$) develop autoimmunity (41, 47). Restoration of ABCA1 function by infusion of APOA-I into *Apoa1*$^{-/-}$ *Ldlr*$^{-/-}$ mice in vivo restored Treg numbers and reduced Teff activation (41). Thus, membrane lipid rafts are critical signaling clusters for T lymphocytes, and modulation of lipid rafts controls much of the T lymphocyte differentiation and activation.

Related to this point above, the development of Tregs and Teffs requires different metabolic checkpoints. mTOR activity is associated with the differential regulation of T cell subsets. Inhibition of cholesterol trafficking in T cells has been shown to inhibit

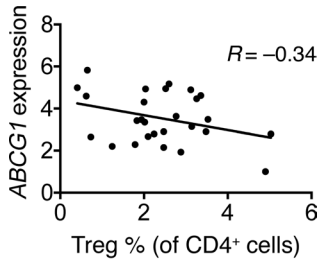

Figure 7. A negative correlation exists between ABCG1 expression and Treg levels in human blood. *ABCG1* mRNA levels from sorted Tregs ($CD4^+CD25^+$) was plotted against the percentage of Tregs ($CD4^+CD25^+CD127^-FOXP3^+$) in the same PBMC sample. PBMCs were prepared from blood drawn from patients in the cardiovascular clinic at the University of Virginia. PBMC samples were divided into 2 portions. One was used for Treg sorting ($CD4^+CD25^+$) and qRT-PCR quantification of ABCG1 levels from sorted Tregs. The other was used for flow cytometric determination of Treg ($CD4^+CD25^+CD127^-FOXP3^+$) percentages. A moderate negative correlation between ABCG1 levels and Treg percentages was observed (R = –0.34). Linear regression was used to determine the association between ABCG1 expression levels and Treg percentages.

mTOR activity. The inhibition of mTOR increases STAT5 phosphorylation and activation, which is critical for Treg development (26–28). In the present study, an increase in both intracellular cholesterol levels and STAT5 phosphorylation were observed in mice in which Tregs lacked ABCG1. Since ABCG1 is essential for intracellular cholesterol distribution, we speculate that cholesterol trafficking is impaired in ABCG1-deficient T cells, which leads to an inhibition of mTOR and in turn enhances STAT5 signaling and Treg differentiation. This is in agreement with a report showing that STAT5 phosphorylation was inhibited by depletion of intracellular cholesterol in erythroid progenitors (48).

Importantly, we found similar associations between Treg frequencies and ABCG1 expression in humans (Figure 7). We measured blood Treg frequencies by flow cytometry and the level of *ABCG1* mRNA expression by quantitative real-time PCR (qRT-PCR) in Tregs isolated from blood of human subjects. We found a significant inverse correlation between Treg frequencies in blood and ABCG1 expression in the human Tregs. The lower the ABCG1 expression in Tregs in human subjects, the higher the Treg frequency, thus supporting our findings in the mouse models. These data suggest that polymorphisms that impact *ABCG1* expression may play a role in regulating atherosclerosis and Treg numbers. Indeed, SNPs in the human *ABCG1* promoter that reduced ABCG1 levels reduced cardiovascular risk, although these studies only focused on macrophages (49, 50). It would be interesting for future studies to address whether there is a negative relationship between *ABCG1* expression in Tregs and the extent of atherosclerosis in humans.

In summary, our results show that Treg differentiation is preferentially increased by the accumulation of cholesterol. This is the first direct evidence to our knowledge that intracellular cholesterol homeostasis affects Treg development. The increase in Treg numbers due to ABCG1 deficiency was sufficient to significantly reduce atherogenesis in mice. We also report here a similar inverse association between ABCG1 expression and Treg frequencies in a small-scale human study. Our data provide new ideas for the potential treatment of atherosclerosis involving the modification of intracellular cholesterol levels and/or ABCG1 expression to regulate Treg development. Additionally, our study provides further clues supporting the notion that the manipulation of cholesterol content in T cells can control their signaling and fates.

Methods

Mice. *Abcg1*$^{fl/fl}$ mice created on a C57Bl/6 background (generated by our laboratory using Ingenious Targeting Laboratory services and previously referenced [16]) were crossed with *Lck-Cre* mice (catalog 003802; The Jackson Laboratory) to obtain *Lck-Cre*$^+$ *Abcg1*$^{fl/fl}$ and control *Lck-Cre*$^-$ *Abcg1*$^{fl/fl}$ mice. *Lck-Cre*$^+$ *Abcg1*$^{fl/fl}$ and control *Lck-Cre*$^-$ *Abcg1*$^{fl/fl}$ mice were subsequently crossed onto the *Ldlr*$^{-/-}$ background (catalog 002207; The Jackson Laboratory) to create *Lck-Cre*$^+$ *Abcg1*$^{fl/fl}$ *Ldlr*$^{-/-}$ and control *Lck-Cre*$^-$ *Abcg1*$^{fl/fl}$ *Ldlr*$^{-/-}$ mice for atherosclerosis studies. *Abcg1*$^{fl/fl}$ mice were crossed with *Foxp3-Cre* mice (catalog 016959; The Jackson Laboratory) and subsequently crossed onto the *Ldlr*$^{-/-}$ background to create *Foxp3-Cre*$^+$ *Abcg1*$^{fl/fl}$ *Ldlr*$^{-/-}$ mice. *Foxp3-Cre*$^+$ *Ldlr*$^{-/-}$ mice were used as controls for the *Foxp3-Cre*$^+$ *Abcg1*$^{fl/fl}$ *Ldlr*$^{-/-}$ mouse studies. All mice used were 8- to 10-week-old females. Mice were fed a standard rodent chow diet containing 0% cholesterol and 5% calories from fat (catalog 5053; Pico Labs). For atherosclerosis studies, mice were fed a high-cholesterol diet containing 1.25% cholesterol and 40% calories from fat (D12108C; Research Diets) for 15 weeks, starting at 8 to 10 weeks of age. Mice were housed in microisolator cages in a pathogen-free animal facility at the La Jolla Institute for Allergy and Immunology.

Immunoblotting. $CD4^+$ cells were isolated from mouse thymus and spleen via magnetic separation (Miltenyi Biotec) and lysed with radioimmunoprecipitation assay (RIPA) buffer (50 mM Tris, pH 7.4, 150 mM NaCl, 1 mM EDTA, 1 mM EGTA, 1 mM $NaVO_4$, 1 mM NaF, 0.5% NP40, 0.1% Brij35, 0.1% deoxycholic acid) and ultrasonication. Protein quantification was performed using BCA Protein Assay Reagent (Thermo Fisher Scientific). Forty-five milligrams protein per

Table 1. Characteristics of human subjects

Patients' characteristics	Cohort	%
Number of subjects	25	
Women	10	40.0%
Men	15	60.0%
White	25	100.0%
African-American	0	0.0%
Hispanic	0	0.0%
Non-Hispanic	25	100.0%
Median age (yr)		
Women	62.0 (48–75)	
Men	69.0 (40–80)	
Median BMI (kg/m)	28.8 (17.2–50.0)	
Lipid Medication, *n* (%)	20	80.0%
LDL cholesterol, mg/dl	76.0 (58–166)	
HDL cholesterol, mg/dl	37.0 (19–71)	
Triglycerides, mg/dl	81 (51–396)	
Maximum stenosis in coronary artery (%)	80% (0%–100%)	

sample was loaded into SDS-PAGE and sequentially immunoblotted with anti-ABCG1 Ab (1:500; catalog NB400-132; Novus Biologicals).

Flow cytometry. Spleens, para-aortic LNs, peripheral LNs (cervical, axillary, brachial, and inguinal), or thymi were excised and pushed through a 40-μm strainer. Red blood cells were lysed in RBC Lysis Buffer according to the manufacturer's protocol (BioLegend). All samples were collected in Dulbecco's PBS (Life Technologies, Thermo Fisher Scientific) with 2 mM EDTA and were stored on ice during staining and analysis. Cells ($2–6 \times 10^6$) were resuspended in 100 μl flow cytometric staining buffer (1% FBS plus 0.1% NaN_3 in PBS). Fc receptors were blocked for 10 minutes, and surface antigens were stained for 30 minutes at 4°C and washed twice with flow cytometric staining buffer. LIVE/DEAD Yellow Fixable Dead Cell Stain (Life Technologies, Thermo Fisher Scientific) was used for analysis of viability, and forward- and side-scatter parameters were used for exclusion of doublets from analysis. Cellular fluorescence was assessed using an LSR II Flow Cytometer (BD Biosciences), and percentages of subsets and MFI were analyzed with FlowJo software, versions 9 and 10.0.8.

For intracellular staining of FOXP3, Ki67, and caspase 3, after surface staining, cells were fixed and made permeable with the Cytofix/Cytoperm Fixation/Permeabilization Solution Kit (BD Biosciences) following the manufacturer's instructions. Cells were stained for 30 minutes at 4°C with Abs and washed twice with the permeabilization buffer.

For intracellular staining of cytokines (IL-10, IL-17, and IFN-γ), cells were incubated with PMA (30 ng/ml) and ionomycin (500 ng/ml) in RPMI Media 1640 (Life Technologies, Thermo Fisher Scientific) supplemented with 10% FBS and antibiotics for 4 hours at 37°C to stimulate cytokine production. GolgiPlug (1 μl/ml; BD Biosciences) was also added to the media to block cytokine secretion.

For evaluation of apoptosis, after surface marker staining, cells were stained with Alexa Fluor 647–conjugated annexin V (1:20 dilution; Life Technologies, Thermo Fisher Scientific) for 15 minutes at room temperature and washed twice. Propidium iodide was added to the staining buffer (1 mg/ml) during resuspension, and the samples were analyzed by flow cytometry within 2 hours of staining.

For measurement of membrane cholesterol, after surface marker staining, cells were stained for an additional 45 minutes at room temperature with 50 mg/ml Filipin III (Cayman) and then washed twice with PBS. The samples were analyzed immediately after staining. For lipid raft staining, the Vybrant Alexa Fluor 594 Lipid Raft Labeling Kit was used according to manufacturer's instructions (Thermo Fisher Scientific).

The following fluorescence-labeled Abs were used: anti-CD4 (clone RM4-5; eBioscience); anti-CD8 (clone RPA-T8; eBioscience); anti-CD25 (clone PC61.5; eBioscience); anti-CD44 (clone IM7; BioLegend); anti-CD62L (clone MEL-14; BioLegend); anti-TCRβ (clone H57-597; eBioscience); anti–PD-1 (clone RMP1-30; eBioscience); anti-CD45.1 (clone A20; eBioscience); anti-CD45.2 (clone 104; eBioscience); anti-FOXP3 (clone FJK-16s; eBioscience); anti–IFN-γ (clone XMG1.2; BD Biosciences); anti–IL-17 (clone eBio17B7; eBioscience); anti–IL-10 (clone JES5-16A3; eBioscience); anti-Ki67 (clone SolA15; eBioscience); and anti–caspase 3 (clone C92-605; BD Biosciences).

Phospho-flow cytometry. Cells were isolated from mouse LNs and stimulated with 100 U/ml recombinant IL-2 (PeproTech) for 15 minutes at 37°C. Immediately following stimulation, cells were stained with surface stain on ice, followed by fixation and permeabilization and staining for FOXP3 and phosphorylated proteins. Lyse/Fix and Perm III buffers (BD Biosciences) were used for intracellular staining of phosphorylated proteins. The following Abs were used for phosphorylated proteins: antiphosphorylated S6 (anti–p-S6) (catalog 5316; Cell Signaling Technology) and anti–p-STAT5 (pY694; BD Biosciences).

In vivo proliferation assay. Mice were injected i.p. with 1 mg BrdU (BD Biosciences). Spleens were harvested after 3 days, and BrdU incorporation was detected following the manufacturer's instructions (BrdU Flow Kit; BD Biosciences).

Bone marrow chimera generation. Recipient CD45.1/2 heterozygous B6.SJL mice were irradiated with 2 doses of 5 Gy each (for a total of 10 Gy) 4 hours apart. Bone marrow cells from both femurs and tibiae of B6.SJL (CD45.1) and *Lck-Cre*$^+$ *Abcg1*$^{fl/fl}$ donor mice were collected under sterile conditions. Bones were centrifuged for the collection of marrow, and the cells were washed and resuspended in PBS for injection. Bone marrow cells from B6.SJL (CD45.1) and *Lck-Cre*$^+$ *Abcg1*$^{fl/fl}$ mice mixed at a 1:1 ratio (4×10^6 cell from each genotype) and in 150 μl PBS were retro-orbitally delivered into each recipient mouse. The ratio of the bone marrow cells was confirmed by flow cytometry. Recipient mice were housed in a barrier facility under pathogen-free conditions and were provided autoclaved acidified water with antibiotics (trimethoprim-sulfamethoxazole) and fed autoclaved food. Ten weeks after the injection, the T cell composition of the chimeric mice was analyzed by flow cytometry.

Atherosclerosis quantification. Mouse aortae were collected and immersed in paraformaldehyde and stained with oil red O, opened longitudinally, and pinned (22). Images were scanned, and the percentage of surface areas occupied by lesions was determined with ImageJ software (NIH).

In vitro Treg differentiation. Naive CD4$^+$CD62L$^+$ T cells were isolated from pooled spleen and peripheral LNs via magnetic separation (Miltenyi Biotec). Cells were then plated at 1×10^5 cells per well in a 96-well U-bottomed plate. Cells were stimulated with Dynabeads Mouse T-Activator CD3/CD28 Beads (Invitrogen) at a ratio of 1 bead to 1 cell. Recombinant TGF-β (2 ng/ml; Peprotech) was added to the culture. Four days later, cells were removed from beads, stained for Treg markers, and analyzed by flow cytometry.

Adoptive transfer. Naive CD4$^+$CD62L$^+$ T cells were isolated from pooled spleens and peripheral LNs from donor mice via magnetic separation (Miltenyi Biotec). Naive cells from C57BL/6J mice on a CD45.1 background (catalog 002014; The Jackson Laboratory) and *Lck-Cre*$^+$ *Abcg1*$^{fl/fl}$ (CD45.2) mice were mixed at a 1:1 ratio (2×10^6 cells from each genotype) and in 150 μl PBS were retro-orbitally delivered into each recipient *Rag1*$^{-/-}$ mouse (catalog 002216; The Jackson Laboratory). The ratio of naive CD4 cells was confirmed by flow cytometry. Ten days after the injection, the T cell composition of the recipient mice was analyzed by flow cytometry.

Treg suppression assay. Naive CD4$^+$CD62L$^+$ T cells were isolated from splenocytes from C57BL/6J mice on a CD45.1 background via magnetic separation (Miltenyi Biotec) and labeled with 5 μM CellTrace Violet according to the manufacturer's protocol (Life Technologies, Thermo Fisher Scientific). CD4-depleted splenocytes were purified from C57BL6/J mice via magnetic separation (Miltenyi Biotec) and irradiated at 30 Gy and used as feeder cells. Tregs from *Lck-Cre*$^+$ *Abcg1*$^{fl/fl}$ *Ldlr*$^{-/-}$ and *Lck-Cre*$^-$ *Abcg1*$^{fl/fl}$ *Ldlr*$^{-/-}$ mice were isolated by FACS sorting of CD4$^+$CD25^{hi} cells from pools of spleens and peripheral LNs. Labeled naive T cells (1.25×10^5) and feeder cells (1×10^6) were cocultured with Tregs (0.78 to 1.25×10^5) in the presence of 2.5 μg/ml anti-mouse CD3 Ab for 3 days. Cell division of naive T cells was quantified as CellTrace Violet dilution by flow cytometry.

Quantitative RT-PCR. Tregs from *Foxp3-Cre*$^{+}$ *Abcg1*$^{fl/fl}$ *Ldlr*$^{-/-}$ and *Foxp3-Cre*$^{+}$ *Ldlr*$^{-/-}$ mice were sorted as CD4^{+}CD25^{hi} cells from blood. Total RNA was extracted by TRIzol (Life Technologies), and cDNA was synthesized with an iScript cDNA Synthesis Kit (Bio-Rad). mRNA expression was measured with qRT-PCR using predesigned TaqMan gene expression assays for *Abcg1* (Mm00437390_m1; Applied Biosystems). Threshold cycles (Ct) were determined by an in-program algorithm assigning a fluorescence baseline based on readings prior to exponential amplification. Fold change in expression was calculated using the ΔΔCt method with *Gapdh* as an endogenous control. The expression level of *Foxp3-Cre*$^{+}$ *Ldlr*$^{-/-}$ Tregs was set at 1.

Human blood analysis. Twenty-five human blood samples were collected at the University of Virginia Cardiac Catheterization Laboratory. Enrolled research participants included both men and women, aged 40–80 years, who presented for a medically necessary cardiac catheterization (15 men and 10 women, average age of 64.6 ± 0.4 years; see Table 1 for a general characterization of the human subjects group studied). Blood was drawn into tubes containing EDTA. Peripheral blood mononuclear cells (PBMCs) were isolated with Ficoll-Paque PLUS (GE Healthcare Life Sciences) and SepMate tubes (STEMCELL Technologies). For ABCG1 expression in Tregs, CD4^{+}CD25^{hi} cells were sorted from PBMCs and subjected to qRT-PCR analysis, as described above, with a TaqMan gene expression assay for human *ABCG1* (Hs00245154_m1; Applied Biosystems). *HPRT1* was used as an endogenous control. For Treg percentages, Tregs were identified as CD4^{+}CD25^{+}CD127^{-}FOXP3^{+} cells by flow cytometry. The following fluorescence-labeled Abs were used: anti-CD4 (clone OKT4; Tonbo Biosciences); anti-CD25 (clone BC96; Tonbo Biosciences); anti-CD127 (clone A019D5; BioLegend); and anti-FOXP3 (clone PCH101; eBioscience).

Plasma lipoprotein measurements. Plasma cholesterol and triglycerides were measured using fast protein liquid chromatography (FPLC) as described previously (16, 51, 52). Equal volumes of plasma from 5 mice per group were pooled, and 200 μl of this pooled plasma was applied to a set of 2 Superose 6 (HR 10/30) columns (GE Healthcare Life Sciences) linked in series. Lipoproteins were eluted by size exclusion into 0.5-ml fractions in EDTA, NaCl, and NaN_3 (1 mmol/l, 0.154 mmol/l, 0.02%) at a flow rate of 0.5 ml/minute. Cholesterol was measured in each fraction using an enzymatic cholesterol kit (Wako Chemicals USA) according to the manufacturer's instructions.

Statistics. All results are expressed as the mean ± SEM. Results were analyzed by Student's *t* test or ANOVA. The unpaired 2-tailed Student's *t* test and 1-way ANOVA were used for comparisons of experimental groups. A *P* value of less than 0.05 was considered statistically significant. Linear regression was used to determine the strength of association between Treg percentages and ABCG1 expression in the human study. An *R* value between –0.5 and –0.3 was considered a moderate association. Statistical analysis was performed using GraphPad Prism software, version 6 (GraphPad Software).

Study approval. Animal use was approved by the La Jolla Institute for Allergy and Immunology and followed NIH guidelines (*Guide for the Care and Use of Laboratory Animals*. National Academies Press. 2011). All experiments were approved by the La Jolla Institute for Allergy and Immunology Animal Care and Use Committee. Informed consent was obtained from human subjects for the use of blood samples, with the approval of the Institutional Review Board for Health Sciences Research at the University of Virginia.

Author contributions

HYC and DEG designed research studies, conducted experiments, acquired and analyzed data, and wrote the manuscript. RW, CM, and LDH conducted experiments. AMT, CAM, and MST designed research. CCH designed research studies and edited the manuscript.

Acknowledgments

The authors would like to thank Jennifer Pattison and Joseph Witztum (UCSD, La Jolla, California, USA) for assistance with the FPLC analysis of plasma lipoproteins; Deborah Yoakum (La Jolla Institute for Allergy and Immunology) for mouse breeding and genotyping; and Frances Gilbert (University of Virginia) for recruitment of human subjects. The authors would also like to thank Antoine Marcais and Thierry Walzer (INSERM, Paris, France) for helpful suggestions on phospho-flow techniques. This work was supported by an American Diabetes Association grant (ADA 7-12-MN-31, to CCH, DEG, and HYC); an American Diabetes Association Award (1-13-MUI-02, to LDH and CCH); NIH grants (F31 HL110668, to LDH; P01 HL055798, to CCH, CAM, and AMT; and R01HL112276-04, to CCH and MST); and American Heart Association grants (AHA 13POST14660055, to HYC and 13POST16990031, to DEG).

Address correspondence to: Catherine C. Hedrick, La Jolla Institute for Allergy and Immunology, 9420 Athena Circle, La Jolla, California 92037, USA. Phone: 858.752.6500; E-mail: Hedrick@lji.org.

Hsin-Yuan Cheng's present address is: Compugen Inc., South San Francisco, California, USA.

LaTeira D. Haynes's present address is: Los Angeles Unified School District, Los Angeles, California, USA.

1. Ward JR, Wilson HL, Francis SE, Crossman DC, Sabroe I. Translational mini-review series on immunology of vascular disease: inflammation, infections and Toll-like receptors in cardiovascular disease. *Clin Exp Immunol*. 2009;156(3):386–394.
2. Robinson JG, Gidding SS. Curing atherosclerosis should be the next major cardiovascular prevention goal. *J Am Coll Cardiol*. 2014;63(25 Pt A):2779–2785.
3. Witztum JL, Lichtman AH. The influence of innate and adaptive immune responses on atherosclerosis. *Annu Rev Pathol*. 2014;9:73–102.
4. Xie JJ, et al. The Th17/Treg functional imbalance during atherogenesis in ApoE(-/-) mice. *Cytokine*. 2010;49(2):185–193.
5. Nilsson J, Wigren M, Shah PK. Regulatory T cells and the control of modified lipoprotein autoimmunity-driven atherosclerosis. *Trends Cardiovasc Med*. 2009;19(8):272–276.
6. Ait-Oufella H, et al. Natural regulatory T cells control the development of atherosclerosis in mice. *Nat Med*. 2006;12(2):178–180.
7. Mallat Z, Ait-Oufella H, Tedgui A. Regulatory T cell responses: potential role in the control of atherosclerosis. *Curr Opin Lipidol*. 2005;16(5):518–524.
8. Yvan-Charvet L, et al. Increased inflammatory gene expression in ABC transporter-deficient macrophages: free cholesterol accumulation, increased signaling via toll-like receptors, and neutrophil infiltration of atherosclerotic lesions. *Circulation*. 2008;118(18):1837–1847.
9. Wang N, Ranalletta M, Matsuura F, Peng F, Tall AR. LXR-induced redistribution of ABCG1 to plasma membrane in macrophages enhances cholesterol mass efflux to HDL. *Arterioscler Thromb Vasc Biol*. 2006;26(6):1310–1316.
10. Gombos I, Kiss E, Detre C, László G, Matkó J.

Cholesterol and sphingolipids as lipid organizers of the immune cells' plasma membrane: their impact on the functions of MHC molecules, effector T-lymphocytes and T-cell death. *Immunol Lett*. 2006;104(1-2):59–69.
11. Goldstein JL, Brown MS. The LDL receptor. *Arterioscler Thromb Vasc Biol*. 2009;29(4):431–438.
12. Wójcicka G, Jamroz-Wiśniewska A, Horoszewicz K, Bełtowski J. Liver X receptors (LXRs). Part I: structure, function, regulation of activity, and role in lipid metabolism. *Postepy Hig Med Dosw (Online)*. 2007;61:736–759.
13. Bensinger SJ, et al. LXR signaling couples sterol metabolism to proliferation in the acquired immune response. *Cell*. 2008;134(1):97–111.
14. Armstrong AJ, Gebre AK, Parks JS, Hedrick CC. ATP-binding cassette transporter G1 negatively regulates thymocyte and peripheral lymphocyte proliferation. *J Immunol*. 2010;184(1):173–183.
15. Sag D, et al. ATP-binding cassette transporter G1 intrinsically regulates invariant NKT cell development. *J Immunol*. 2012;189(11):5129–5138.
16. Sag D, Cekic C, Wu R, Linden J, Hedrick CC. The cholesterol transporter ABCG1 links cholesterol homeostasis and tumour immunity. *Nat Commun*. 2015;6:6354.
17. Hennet T, Hagen FK, Tabak LA, Marth JD. T-cell-specific deletion of a polypeptide N-acetylgalactosaminyl-transferase gene by site-directed recombination. *Proc Natl Acad Sci USA*. 1995;92(26):12070–12074.
18. Mombaerts P, Iacomini J, Johnson RS, Herrup K, Tonegawa S, Papaioannou VE. RAG-1-deficient mice have no mature B and T lymphocytes. *Cell*. 1992;68(5):869–877.
19. Kong KF, et al. Protein kinase C-η controls CTLA-4-mediated regulatory T cell function. *Nat Immunol*. 2014;15(5):465–472.
20. Packard RR, Maganto-García E, Gotsman I, Tabas I, Libby P, Lichtman AH. CD11c(+) dendritic cells maintain antigen processing, presentation capabilities, and CD4(+) T-cell priming efficacy under hypercholesterolemic conditions associated with atherosclerosis. *Circ Res*. 2008;103(9):965–973.
21. Maganto-García E, Tarrio ML, Grabie N, Bu DX, Lichtman AH. Dynamic changes in regulatory T cells are linked to levels of diet-induced hypercholesterolemia. *Circulation*. 2011;124(2):185–195.
22. Cheng HY, Wu R, Hedrick CC. Gammadelta (γδ) T lymphocytes do not impact the development of early atherosclerosis. *Atherosclerosis*. 2014;234(2):265–269.
23. Gotsman I, et al. Impaired regulatory T-cell response and enhanced atherosclerosis in the absence of inducible costimulatory molecule. *Circulation*. 2006;114(19):2047–2055.
24. Herbin O, et al. Regulatory T-cell response to apolipoprotein B100-derived peptides reduces the development and progression of atherosclerosis in mice. *Arterioscler Thromb Vasc Biol*. 2012;32(3):605–612.
25. Li X, Zheng Y. Regulatory T cell identity: formation and maintenance. *Trends Immunol*. 2015;36(6):344–353.
26. Michalek RD, et al. Cutting edge: distinct glycolytic and lipid oxidative metabolic programs are essential for effector and regulatory CD4+ T cell subsets. *J Immunol*. 2011;186(6):3299–3303.
27. Zeng H, Yang K, Cloer C, Neale G, Vogel P, Chi H. mTORC1 couples immune signals and metabolic programming to establish T(reg)-cell function. *Nature*. 2013;499(7459):485–490.
28. Xu J, Dang Y, Ren YR, Liu JO. Cholesterol trafficking is required for mTOR activation in endothelial cells. *Proc Natl Acad Sci USA*. 2010;107(10):4764–4769.
29. Sturek JM, et al. An intracellular role for ABCG1-mediated cholesterol transport in the regulated secretory pathway of mouse pancreatic beta cells. *J Clin Invest*. 2010;120(7):2575–2589.
30. Tarling EJ, Edwards PA. ATP binding cassette transporter G1 (ABCG1) is an intracellular sterol transporter. *Proc Natl Acad Sci USA*. 2011;108(49):19719–19724.
31. Leventhal AR, Chen W, Tall AR, Tabas I. Acid sphingomyelinase-deficient macrophages have defective cholesterol trafficking and efflux. *J Biol Chem*. 2001;276(48):44976–44983.
32. Antov A, Yang L, Vig M, Baltimore D, Van Parijs L. Essential role for STAT5 signaling in CD25+CD4+ regulatory T cell homeostasis and the maintenance of self-tolerance. *J Immunol*. 2003;171(7):3435–3441.
33. Passerini L, et al. STAT5-signaling cytokines regulate the expression of FOXP3 in CD4+CD25+ regulatory T cells and CD4+CD25- effector T cells. *Int Immunol*. 2008;20(3):421–431.
34. Shan J, et al. Interplay between mTOR and STAT5 signaling modulates the balance between regulatory and effective T cells. *Immunobiology*. 2015;220(4):510–517.
35. Marçais A, et al. The metabolic checkpoint kinase mTOR is essential for IL-15 signaling during the development and activation of NK cells. *Nat Immunol*. 2014;15(8):749–757.
36. Tall AR, Yvan-Charvet L, Terasaka N, Pagler T, Wang N. HDL, ABC transporters, and cholesterol efflux: implications for the treatment of atherosclerosis. *Cell Metab*. 2008;7(5):365–375.
37. McCarthy C, et al. IL-10 mediates the immunoregulatory response in conjugated linoleic acid-induced regression of atherosclerosis. *FASEB J*. 2013;27(2):499–510.
38. Terkeltaub RA. IL-10: An "immunologic scalpel" for atherosclerosis?. *Arterioscler Thromb Vasc Biol*. 1999;19(12):2823–2825.
39. Pinderski Oslund LJ, et al. Interleukin-10 blocks atherosclerotic events in vitro and in vivo. *Arterioscler Thromb Vasc Biol*. 1999;19(12):2847–2853.
40. Uyemura K, et al. Cross-regulatory roles of interleukin (IL)-12 and IL-10 in atherosclerosis. *J Clin Invest*. 1996;97(9):2130–2138.
41. Wilhelm AJ, et al. Apolipoprotein A-I modulates regulatory T cells in autoimmune LDLr-/-, ApoA-I-/- mice. *J Biol Chem*. 2010;285(46):36158–36169.
42. Waddington KE, Jury EC. Manipulating membrane lipid profiles to restore T-cell function in autoimmunity. *Biochem Soc Trans*. 2015;43(4):745–751.
43. Kidani Y, et al. Sterol regulatory element-binding proteins are essential for the metabolic programming of effector T cells and adaptive immunity. *Nat Immunol*. 2013;14(5):489–499.
44. Terasaka N, et al. ABCG1 and HDL protect against endothelial dysfunction in mice fed a high-cholesterol diet. *J Clin Invest*. 2008;118(11):3701–3713.
45. Terasaka N, Wang N, Yvan-Charvet L, Tall AR. High-density lipoprotein protects macrophages from oxidized low-density lipoprotein-induced apoptosis by promoting efflux of 7-ketocholesterol via ABCG1. *Proc Natl Acad Sci USA*. 2007;104(38):15093–15098.
46. Bensinger SJ, Tontonoz P. Integration of metabolism and inflammation by lipid-activated nuclear receptors. *Nature*. 2008;454(7203):470–477.
47. Wilhelm AJ, et al. Apolipoprotein A-I and its role in lymphocyte cholesterol homeostasis and autoimmunity. *Arterioscler Thromb Vasc Biol*. 2009;29(6):843–849.
48. McGraw KL, et al. Erythropoietin receptor signaling is membrane raft dependent. *PLoS ONE*. 2012;7(4):e34477.
49. Xu Y, et al. A polymorphism in the ABCG1 promoter is functionally associated with coronary artery disease in a Chinese Han population. *Atherosclerosis*. 2011;219(2):648–654.
50. Liu F, et al. ABCG1 rs57137919G>a polymorphism is functionally associated with varying gene expression and apoptosis of macrophages. *PLoS ONE*. 2014;9(6):e97044.
51. Hanna RN, et al. NR4A1 (Nur77) deletion polarizes macrophages toward an inflammatory phenotype and increases atherosclerosis. *Circ Res*. 2012;110(3):416–427.
52. Hedrick CC, Castellani LW, Warden CH, Puppione DL, Lusis AJ. Influence of mouse apolipoprotein A-II on plasma lipoproteins in transgenic mice. *J Biol Chem*. 1993;268(27):20676–20682.